

Influence of secondary carbides precipitation and transformation on the secondary hardening of laser melted high chromium steel

Yong Wang · Mei Yan Li · Bin Han ·
Tao Han · Yi Yuan Cheng

Received: 14 November 2009 / Accepted: 1 March 2010 / Published online: 14 March 2010
© Springer Science+Business Media, LLC 2010

Abstract The influence of secondary carbides precipitation and transformation on the secondary hardening of laser melted high chromium steels was analyzed by means of scanning electron microscopy, transmission electron microscopy, and X-ray diffraction. The microstructure of laser melted high chromium steel is composed of austenite with supersaturated carbon and alloy elements and granular interdendritic carbides of type $M_{23}C_6$. Secondary hardening of the laser melted layer begins at 450 °C after tempering, and the hardness reaches a peak of 672HV at 560 °C and then decreases gradually. After tempering at 560 °C, a large amount of lamellar martensite was formed in the laser melted layer with a small quantity of thin lamellar M_3C cementite due to the martensitic decomposition. The stripy carbides precipitating at the grain boundaries were determined to be complex hexagonal M_7C_3 carbides and face centered cubic $M_{23}C_6$ carbides. In addition, the granular $M_{23}C_6$ carbides and fine rod-like shaped M_7C_3 carbides coexisted within the dendrites. As a result, the combined effects of martensitic transformation, ultrafine carbide precipitations, and dislocation strengthening result in the secondary hardening of the laser melted layer when the samples were tempered at 560 °C.

Introduction

High chromium steels have been considered candidate materials for wear-resistance components in mining and

materials industry because of their excellent abrasion resistance imparted by the hard eutectic alloy carbides present in the microstructure [1]. However, reticular brittle carbides precipitated along the grain boundaries (GBs) are quite stable and are difficult to change by heat treatment. The casting subjected to conventional heat treatment trends to crack due to the poor thermal conductivity of high chromium steels. Especially, the zonal distribution of carbides reduces ductility and limits the application of high chromium steels.

In recent years, advanced rapid solidification technologies such as surface melting employing laser beam and electron beam have been reported to be feasible routes for enhancing the surface properties of high carbon and alloy steels [2–6]. Among these surfacing techniques, laser surface melting (LSM) is the simplest and most economical treatment method. It does not involve change in the overall chemical composition and no additional precious metals are needed. Another advantage of LSM over conventional heat treatment is its capability for localized treatment of a selected part of a surface, leaving the other parts unaffected. Direct irradiation of a solid surface by a laser beam results in rapid melting and solidification with heating and cooling rates up to $10^4 \sim 10^8$ K/s. These rates promote mixing, rapid diffusion and the formation of amorphous and microcrystalline surface layers, which consequently improve mechanical performance of material surfaces. Furthermore, owing to the high cooling rates in LSM, traditional transformations are often inhibited, and instead the molten pool undergoes a non-equilibrium solidification process and a large amount of austenite forms [7, 8].

For many applications, the components are heat-treated prior to service. Especially, adopting the tempering treatment reduces cost and avoids distortion and fissuring of the

Y. Wang · M. Y. Li (✉) · B. Han · T. Han · Y. Y. Cheng
College of Electromechanical Engineering, China University
of Petroleum, 271 Bei'er Road, Dongying 257061,
Shandong, China
e-mail: lmy_102411@163.com

casting [9]. Until now, several studies on the precipitation and transformation of secondary carbides in the as-cast high carbon and alloy steels have been performed [10–13]. Studies of the tempering behavior of the non-equilibrium microstructures after LSM are scarce, but they have shown that secondary hardening can be achieved and, more importantly, that the hardness and the secondary hardening temperature are higher than after conventional quenching and tempering treatments [14, 15]. Hence, before practical applications further studies of the hardening behavior of the laser melted steels are necessary.

This study aims to give a further insight into the microstructure in the laser melted layer subjected to tempering at the secondary hardening temperature, and to identify the influence of secondary carbides precipitation and transformation on the secondary hardening of laser melted high chromium steels subjected to tempering.

Experimental procedure

As-received high chromium steel with a chemical composition in wt%: 1.09C, 10.48Cr, 1.24Si, 0.53Mn, 0.56Ni, 1.04Mo, 0.39V, 0.031P, 0.017S, balance Fe, was machined to the rectangular shape of 50 × 20 × 10 mm. LSM was performed using a continuous wave CO₂ laser, with argon as shielding gas to minimize oxidation. A laser power of 2.7 kW at the workpiece with a beam size of 3 mm in diameter and beam scanning velocity of 5 mm/s was used. After LSM, the specimens were tempered for 2 h at temperatures of 300–650 °C. For metallographic examination, cross-sections of specimens were polished and etched in 4% nital and in chloroazotic acid, respectively. The microstructure of specimens was observed by scanning electron microscopy (SEM) and transmission electron microscopy (TEM). The phases present in the laser melted and tempered layers were studied by X-ray diffraction (XRD). Vickers microhardness tests were performed with a load of 200 g.

Results and discussion

Microstructure of the laser melted layer

According to the previous work [16], the microstructure of the as-received high chromium steel essentially consists of tempered martensite and a significant quantity of M₇C₃ carbides, as shown in Fig. 1a. In the as-cast condition, the high alloy contents in high chromium steels inherently give rise to carbide segregation at the GBs and a coarse-grained microstructure by conventional casting processing. Consequently, the carbides reduce ductility since they constitute a

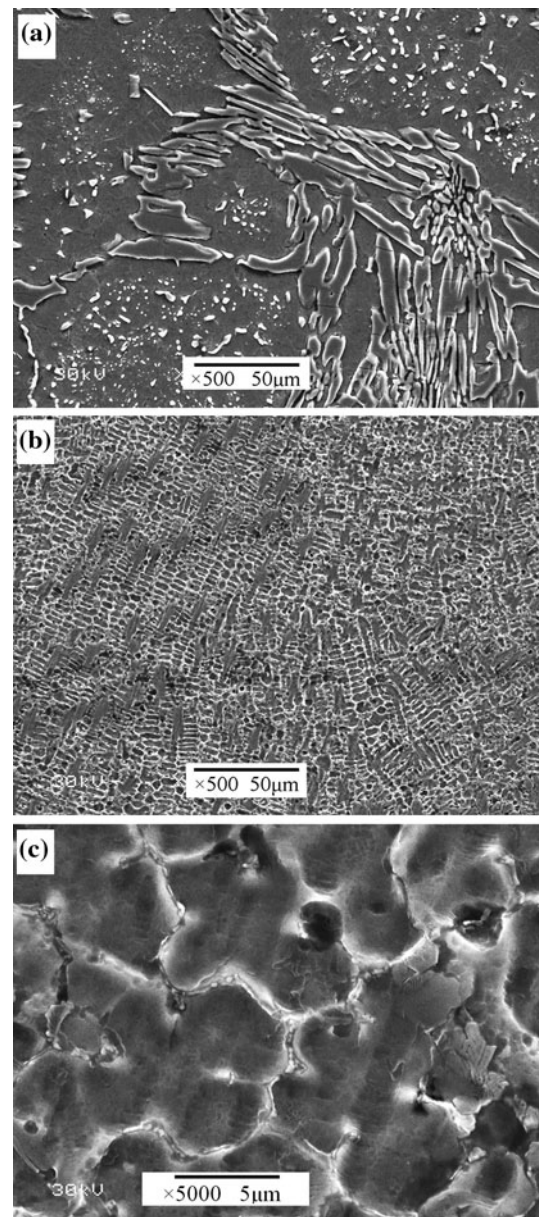


Fig. 1 a SEM micrograph of the as-received high chrome steel, b SEM micrograph of the laser melted layer at low magnification, c at high magnification

favorable propagation path for the mechanical and thermal fatigue cracks [17].

As shown in Fig. 1b, large brittle carbides were completely dissolved and dense ultrafine austenitic dendrites were formed in the melted layer. Ultrafine granular carbides at GBs can be seen at high magnification in Fig. 1c, which are revealed to be face centered cubic (FCC) M₂₃C₆ in the previous work [16]. In this and all similar examples to follow, the capital letter M refers to metallic elements that can form carbides. Typical carbide forming elements include, but are not limited to Fe, Cr, Mo, and V

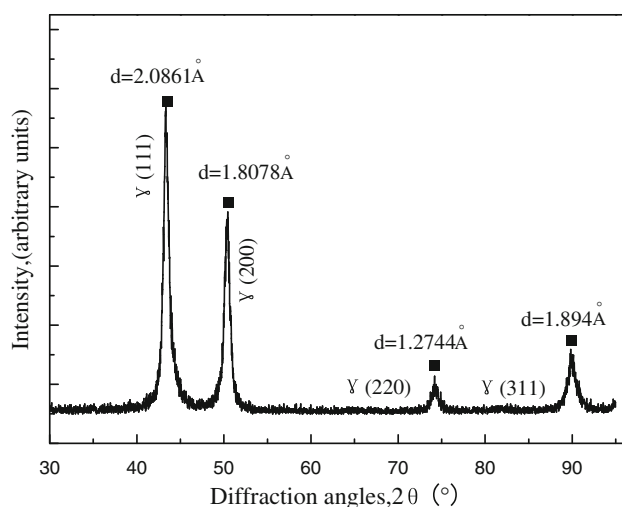


Fig. 2 XRD patterns of the laser melted layer

in this work. Furthermore, the austenite in the melted layer is strengthened by solid solution, dislocations, and ultrafine grains, which are likely to contribute to the relatively high hardness compared with the conventional austenite.

The XRD analysis of laser melted high chromium steel indicates that the microstructure of the melted layer is composed of austenite (Fig. 2). Actually, the mean lattice parameters of the FCC austenite phase amounts to 0.36206 nm with the precision level of 0.00001. Comparison of the experimentally determined d spacings with those given in the standard X-ray powder diffraction data indicates that the lattice parameters of austenite in the melted layer are greater than the normal lattice constant of austenite (0.3585 nm) [18]. The increase of the lattice parameter suggests that a significant dissolution of alloying elements, such as C, Cr, Mo, and V, commenced in the austenite. The existence of austenite may be attributed to the low martensite start (M_s) temperature, the high concentration of austenite stabilizing elements such as Cr, Mo, and V [19].

Secondary hardening during tempering

Hardness curves of the laser melted layers after tempering at different temperatures are shown in Fig. 3. The whole process of secondary hardening can be described in the following four stages: (1) the hardness begins to ascend when tempered at 450 °C, (2) the hardness increases more quickly with tempering temperature higher than 500 °C, (3) the maximum hardness can be obtained after tempering at 560 °C, and (4) when the tempering temperature exceeds 600 °C, the hardness of the laser melted layer descends dramatically.

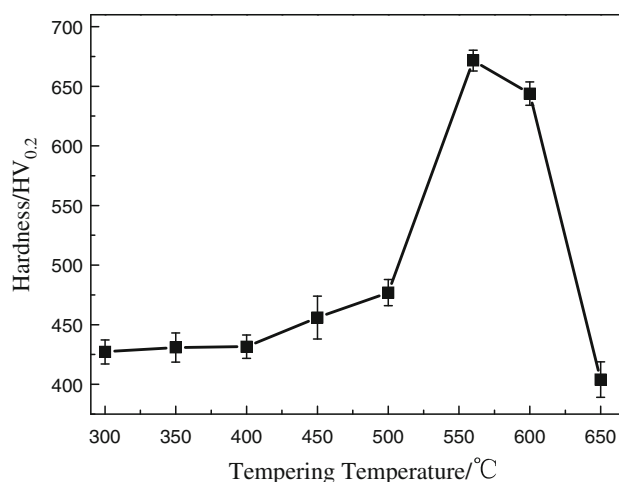


Fig. 3 Hardness of the laser melted layer vs tempering temperature

Effect of phase transformation on the secondary hardening

Secondary carbides precipitation

According to XRD in Fig. 4, the laser melted layer appears to be a mixed martensite–austenite structure after tempering at 560 °C for 2 h, while no carbide peaks are found in XRD patterns due to the low weight percent of carbides. As shown in Fig. 5a, structural characteristics of the laser melted layer after tempering at 560 °C change dramatically compared with those shown in Fig. 1b. It could be noted that fine lamellar carbides are precipitated at the GBs with the thickness of approximately 200–500 nm as shown in Fig. 5b. However, it is difficult to confirm the style and structure of the precipitates by SEM.

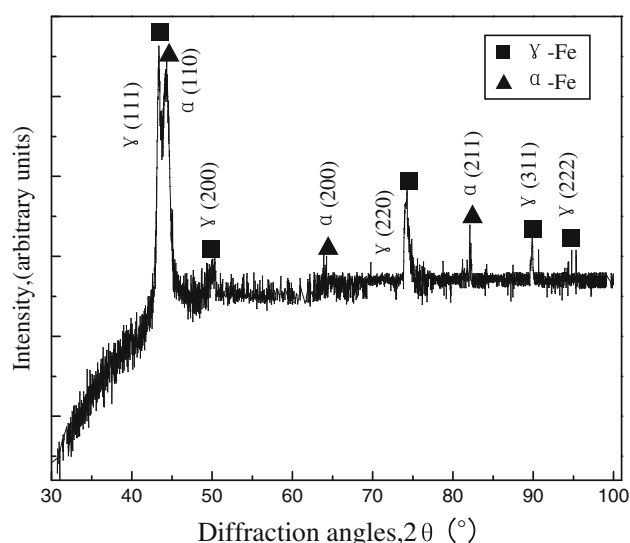


Fig. 4 X-ray diffractograms of the laser melted layer after tempering at 560 °C

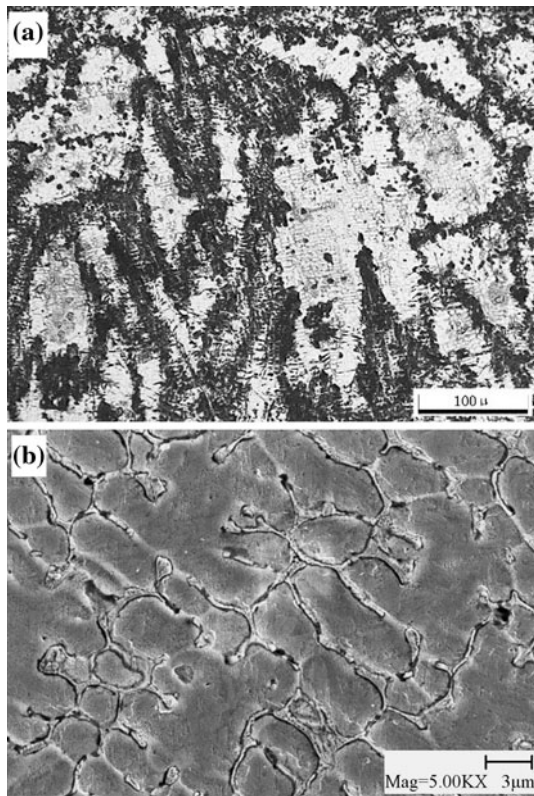


Fig. 5 **a** Optical micrograph at low magnification of the laser melted layer tempered at 560 °C, **b** SEM micrograph of carbides etched in chloroazotic acid

TEM examinations give more information on the secondary hardening carbides. According to the selected area electron diffraction (SAED) pattern in Fig. 6a, these stripy carbides at GBs are determined to be complex hexagonal M_7C_3 carbides (Fig. 6a, b) and FCC $M_{23}C_6$ carbides (Fig. 6c, d). In addition, the fine rod-like shaped M_7C_3 carbides (Fig. 7a, b) and the granular $M_{23}C_6$ carbides (Fig. 7c, d) coexist within the dendrites.

Laser irradiation leads to the complete dissolution of M_7C_3 carbides, and during the subsequent cooling, the increase in the carbon and alloying elements concentration in the solid solution contributes to the greater mean lattice parameter than the normal lattice constant of austenite. As shown in Fig. 3, the austenite has a high tempering stability, while the following reasons can be speculated. (1) The alloying elements preclude solid state transformation of the austenite and inhibit the precipitation and growth of carbides [14]. (2) The alloying elements in the austenite change the size of the interstices of the grains and promote the diffusive activation energy of atoms [15]. These elements will precipitate from the austenite in the form of secondary carbides during tempering at 560 °C. This process is controlled by the diffusion of alloying elements such as Cr, Mo, and V within the austenite. According to

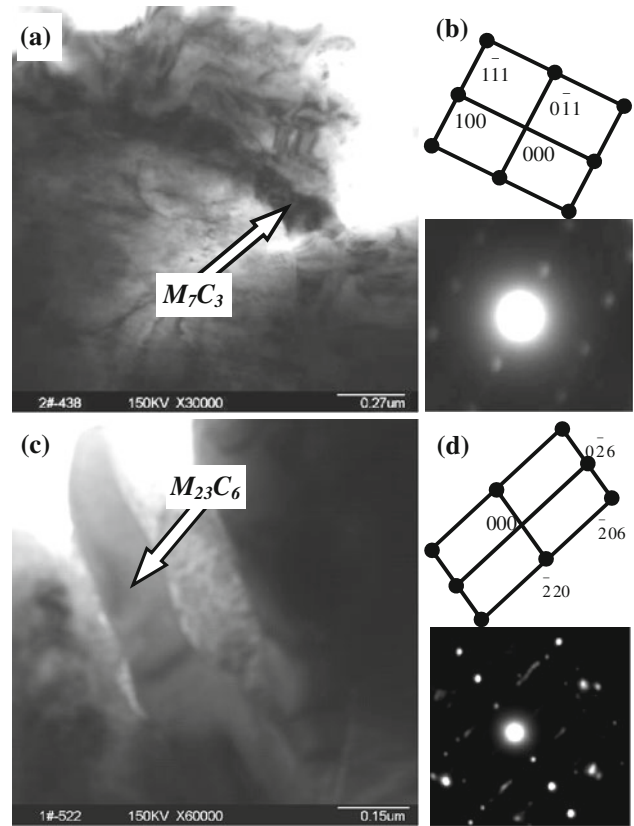


Fig. 6 TEM micrographs of the stripy intragranular carbides **a** M_7C_3 carbides and **b** its SAED patterns, **c** $M_{23}C_6$ carbides and **d** its SAED patterns

the phase diagram of Fe–C–Cr [20], the complex hexagonal M_7C_3 carbide will precipitate from the austenite preferentially, and then the M_7C_3 carbides partially dissolved followed by the precipitation of the $M_{23}C_6$ carbides. Moreover, the another reason for the present of $M_{23}C_6$ carbides is speculated to the direct precipitation from the austenite, which is explained in terms of the good lattice matching between austenite and $M_{23}C_6$ carbides, decreasing the free surface energy and nucleation activation energy [13, 21].

Martensitic transformation

The TEM observation reveals lamellar cryptocrystalline martensite within the austenitic dendrites, as shown in Fig. 8. In addition, morphology and distribution of cementite (M_3C) in the decomposed regions are illustrated in Fig. 9. As it is can be seen, the M_3C carbides are distributed as some parallel rows, probably perpendicular to the lamellar martensite. In this particular case, the thin lamellar orthorhombic M_3C cementite precipitate with a common orientation and the OR between M_3C and martensite is deduced to be Bagaryatsky relationship: $(100)M_3C // (1\bar{1}0)\alpha'$. It is

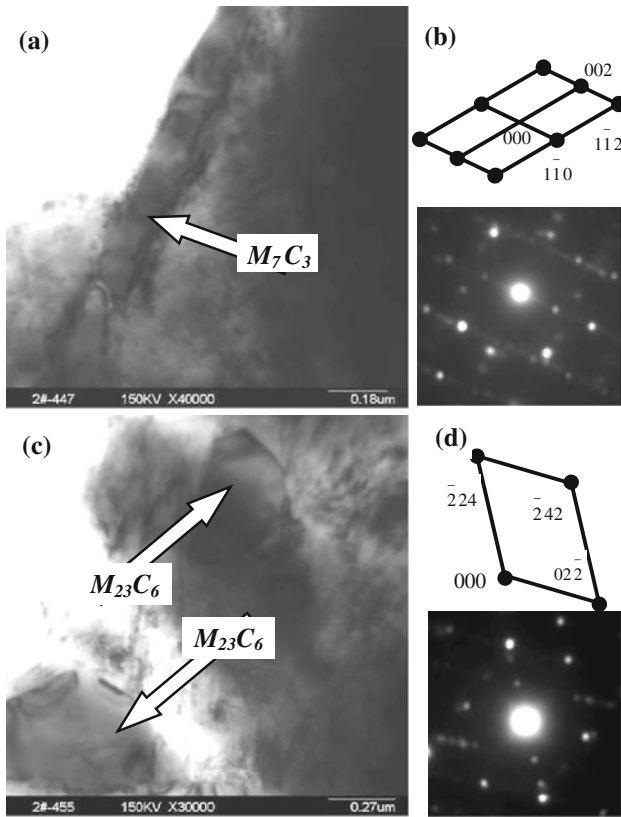


Fig. 7 TEM micrographs of carbides along the grain boundaries **a** fine rod-like shaped M_7C_3 carbides and **b** its SAED patterns, **c** granular $M_{23}C_6$ carbides and **d** its SAED patterns

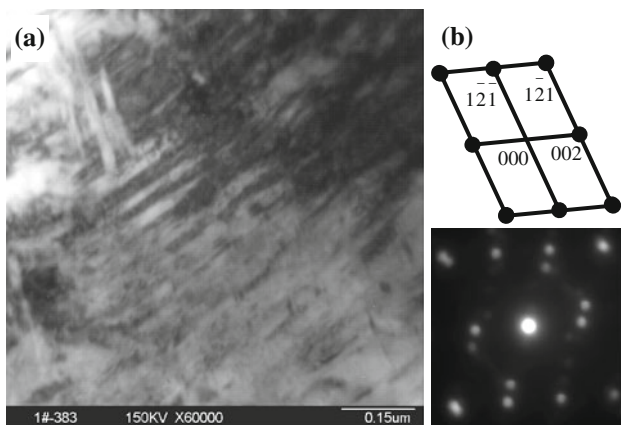


Fig. 8 Cryptocrystalline martensite in the laser melted layer tempered at 560 °C **a** TEM micrograph, **b** the SAED patterns

important to note that thin lamellar M_3C carbides perpendicular to the lamellar martensite are not the results of austenitic decomposition but those of martensite.

Austenite in the laser melted high chromium steel presents a very high dislocation density [15, 16, 22] and, as previously mentioned, it is largely supersaturated in alloying elements. Segregation of interstitial solute atoms

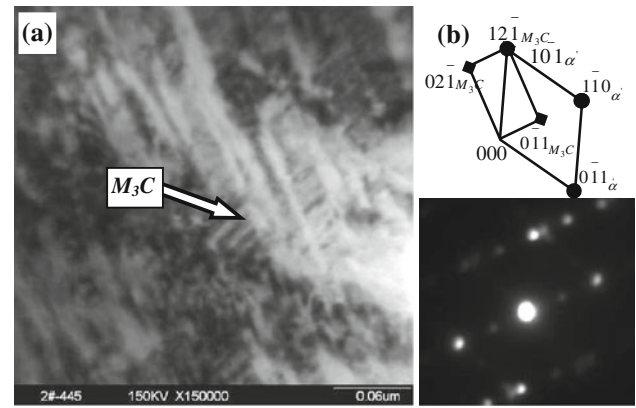


Fig. 9 Lamellar M_3C precipitated inside martensite **a** TEM micrograph, **b** the SAED patterns

to austenite dislocations and to dendritic interfaces contributes significantly to stabilizing austenite [14]. However, after the precipitation of secondary carbide $M_{23}C_6$, the depletion of carbon and chromium contents of matrix increased the M_s temperature of the austenitic matrix during subsequently cooling to ambient temperature. This caused more austenite transform to martensite during air cooling to ambient temperature. Also, the tempering of the laser melted layer, causing a residual stress relief of the material, may also contribute to destabilizing austenite [23] so that the austenite content in the matrix decreased. Both these factors are responsible for the secondary hardening at 560 °C. Consequently, in the laser melted tempered high chromium steels secondary hardening results simultaneously from the $\gamma \rightarrow \alpha$ transformation and the precipitation of carbides within a refined microstructure.

Effect of substructure on secondary hardening

As illustrated in Fig. 10, high-density dislocations and stacking faults are observed within the retained austenite of laser melted layer after tempering at 560 °C. Recovery occurring during reheating caused the density of dislocations to decrease in some degree. However, the dislocations pinned by the precipitates were relatively stable [24]. Thus, the dislocation networks in the austenitic matrix were not completely eliminated by tempering at 560 °C, contributing to the strength of the laser melted high chromium steel. As a result, dislocation strengthening is another important factor for secondary hardening after tempering at 560 °C.

Conclusions

LSM of high chromium steel leads to the complete dissolution of brittle M_7C_3 carbides, and the melted layer consists of austenitic dendrites and interdendritic $M_{23}C_6$

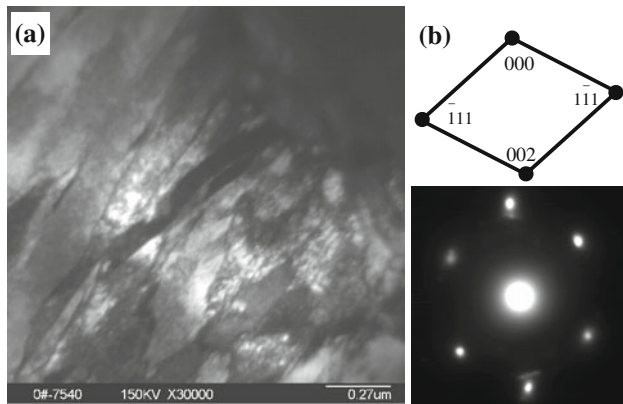


Fig. 10 High-density dislocations inside austenite **a** TEM micrograph, **b** the SAED patterns

carbides particles. The secondary hardening of the laser melted high chromium steel began at 450 °C after tempering; the hardness reached a peak of 672HV at 560 °C and then descended dramatically when the tempering temperature exceeded 600 °C. After tempering at 560 °C, a large amount of lamellar cryptocrystalline martensite was formed in the laser melted layer with a small quantity of thin lamellar M_3C cementite due to the martensitic decomposition. The M_7C_3 and $M_{23}C_6$ carbides precipitating at GBs were determined to be stripy. In addition, the granular $M_{23}C_6$ carbides and fine rod-like shaped M_7C_3 carbides coexisted within the dendrites. Therefore, with secondary carbides precipitating from austenite and martensite forming, the hardness of the laser melted steel increases. Moreover, dislocation strengthening is another important factor for secondary hardening after tempering at 560 °C.

Acknowledgement The authors would like to acknowledge the supports from the Natural Science Foundation of Shandong Province (No. Y2006F4).

References

1. Tabrett CP, Sare IR (1998) *Scr Mater* 38:1747
2. Kac S, Kusinski J (2003) *Mater Chem Phys* 81:510
3. Colaco R, Pina C, Vilar R (1999) *Scr Mater* 41:715
4. Ivanov Yu, Matz W, Rotshtein V, Gunzel R, Shevchenko N (2002) *Surf Coat Technol* 150:188
5. Mei XX, Sun WF, Hao SZ, Ma TC, Dong C (2007) *Surf Coat Technol* 201:5072
6. Uglov VV, Anishchik VM, Astashynski VV, Stalmoshenok EK, Rusalsky DP, Cherenda NN, Rummyanceva IN, Askerko VV, Kuzmitski AM (2004) *Surf Coat Technol* 180–181:108
7. Colaco R, Gordo E, Ruiz-Navas EM, Otasevic M, Vilar R (2006) *Wear* 260:949
8. Abboud JH, Benyounis KY, Olabi AG, Hashmi MSJ (2007) *J Mater Process Technol* 182:427
9. Wang J, Sun ZP, Liu HH, Gao SJ, Shen BL, Huang SJ (2003) *Foundry* 52:1065 (in Chinese)
10. Tabrett CP, Sare IR (1997) *Wear* 203–204:206
11. Powell GLF, Bee JV (1996) *J Mater Sci* 31:707. doi:10.1007/BF00367889
12. Sun Z, Zuo R, Li C, Shen B, Yan J, Huang S (2004) *Mater Charact* 53:403
13. Radulovic M, Fiset M, Peev K, Tomovic M (1994) *J Mater Sci* 29:5085. doi:10.1007/BF01151101
14. Colaco R, Vilar R (1997) *Scr Mater* 38:107
15. Wu Run, Xie Chang-sheng, Hu Mulin, Cai Wei-ping (2000) *Mater Sci Eng A* 278:1
16. Li Meiyuan, Wang Yong, Han Bin, Zhao Weimin, Han Tao (2009) *Appl Surf Sci* 255:7574
17. Li Zhou, Da-le Sun, Chang-sheng Liu, Qiong Wu (2006) *J Iron Steel Res Int* 13:49
18. Liu Hao-huai, Wang Jun, Shen Bao-luo, Yang Hong-shan, Gao Sheng-ji, Huang Si-jiu (2007) *Mater Des* 28:1059
19. Colaco R, Vilar R (2004) *Mater Sci Eng A* 385:123
20. Mlian PA, Rajasekhara HS (1986) *J Mater Sci Lett* 5:1292
21. Wang J, Zuo RL, Sun ZP, Li C, Liu HH, Yang HS, Shen BL, Huang SJ (2005) *Mater Charact* 55:234
22. Vilar R, Colaço R, Almeida A (1995) *Opt Quant Electron* 27:1273
23. Xie ZL, Liu Y, Hanninen H (1994) *Acta Metallurgica et Materialia* 42:4117
24. Wu HB, Jiang HT, Yang SW, Tang D, He XL (2007) *Acta Metall Sin* 20:313